Geophysical Research Letters

RESEARCH ARTICLE
10.1029/2021GL096495

Role of the Deglacial Buildup of the Great Barrier Reef for the Global Carbon Cycle

Thomas Felis[1], **Gustavo Hinestrosa**[2], **Peter Köhler**[3], **and Jody M. Webster**[2]

[1]MARUM – Center for Marine Environmental Sciences, University of Bremen, Bremen, Germany, [2]Geocoastal Research Group, School of Geosciences, The University of Sydney, Sydney, NSW, Australia, [3]Alfred-Wegener-Institut Helmholtz-Zentrum für Polar- und Meeresforschung (AWI), Bremerhaven, Germany

Key Points:

- Great Barrier Reef corals indicate pronounced decrease in skeletal stable carbon isotopes between 12.8 and 11.7 ka during Younger Dryas
- Event follows shelf flooding and barrier reef initiation at 13 ka and coincides with prominent atmospheric stable carbon isotope minimum
- Carbon cycle modeling reveals marginal impact of changes in reef carbonate production and land carbon decomposition on atmospheric carbon

Supporting Information:

Supporting Information may be found in the online version of this article.

Correspondence to:

T. Felis,
tfelis@marum.de

Citation:

Felis, T., Hinestrosa, G., Köhler, P., & Webster, J. M. (2022). Role of the deglacial buildup of the Great Barrier Reef for the global carbon cycle. *Geophysical Research Letters*, *49*, e2021GL096495. https://doi.org/10.1029/2021GL096495

Received 6 OCT 2021
Accepted 11 JAN 2022

Abstract The carbon isotope ^{13}C is commonly used to attribute the last deglacial atmospheric CO_2 rise to various processes. Here we show that the growth of the world's largest reef system, the Great Barrier Reef (GBR), is marked by a pronounced decrease in $\delta^{13}C$ in absolutely dated fossil coral skeletons between 12.8 and 11.7 ka, which coincides with a prominent minimum in atmospheric $\delta^{13}CO_2$ and the Younger Dryas. The event follows the flooding of a large shelf platform and initiation of an extensive barrier reef system at 13 ka. Carbon cycle simulations show the coral $\delta^{13}C$ decrease was mainly caused by the combination of isotopic fractionation during reef carbonate production and the decomposition of organic land carbon on the newly flooded shallow-water platform. The impacts of these processes on atmospheric CO_2 and $\delta^{13}CO_2$, however, are marginal. Thus, the GBR was not contributing to the last deglacial $\delta^{13}CO_2$ minimum at ~12.4 ka.

Plain Language Summary An outstanding problem in our understanding of the global carbon cycle is unraveling the processes that were responsible for the rise of atmospheric CO_2 during the last deglaciation (19,000–11,000 years ago). The carbon isotope ^{13}C is commonly used to attribute the last deglacial atmospheric CO_2 rise to various processes. The growth of tropical coral reefs has been controversially discussed in this context. To test this, well constrained reef carbonate records that span the last deglaciation are necessary, but such records are generally not available. Here we make use of a multi-proxy coral reef record obtained at the Great Barrier Reef (GRB). The $\delta^{13}C$ signal in the carbonate skeletons of fossil corals indicates a pronounced minimum that precisely coincides with a prominent minimum in atmospheric $\delta^{13}CO_2$ as indicated by ice core records for the Younger Dryas cold period. We show, by carbon cycle simulations, that the GBR coral $\delta^{13}C$ signal can be explained by changes in reef carbonate production and decomposition of organic land carbon on a newly flooded wide area. However, the simulations indicate that that the world's largest reef system in existence appears to have little effect on the last deglacial atmospheric CO_2 and $\delta^{13}CO_2$ changes.

1. Introduction

The $\delta^{13}C$ values of atmospheric carbon dioxide (CO_2) reconstructed from ice cores show that during the last deglaciation CO_2 with lower amounts of ^{13}C was released to the atmosphere in two rapid episodes (Bauska et al., 2016; Schmitt et al., 2012). In parallel to the onset of the deglacial CO_2 rise (Figure 1b) a prominent drop in the atmospheric $\delta^{13}CO_2$ values (Figure 1c) leading to a minimum centered at ~16.0 ka is most commonly attributed to upwelling of old ^{13}C-depleted waters in the Southern Ocean (Köhler et al., 2005a; Menviel et al., 2018; Schmitt et al., 2012). However, the cause of a second prominent minimum in atmospheric $\delta^{13}CO_2$ centered at ~12.4 ka during the Northern Hemisphere's Younger Dryas cold period (Figures 1a and 1c) that is synchronous to another period of CO_2 rise is not well understood (Bauska et al., 2016; Schmitt et al., 2012). Multi-proxy evidence invoke another pulse of Southern Ocean upwelling to explain these late deglacial carbon cycle changes (Anderson et al., 2009; Marchitto et al., 2007; Marcott et al., 2014; Ronge et al., 2020; Skinner et al., 2010), others suggest the upwelling of carbon rich waters in the Pacific (Shuttleworth et al., 2021), or some marine or terrestrial contributions caused by a weakening of the Atlantic meridional overturning circulation during the Younger Dryas (Bauska et al., 2016; Böhm et al., 2015; Gottschalk et al., 2019; Köhler et al., 2005a). A similar pattern as that reconstructed for $\delta^{13}CO_2$ values has been observed for marine $\delta^{13}C$ records of surface and thermocline waters (Lynch-Stieglitz et al., 2019) and was interpreted as an imprint of the atmospheric $\delta^{13}CO_2$ changes on the $\delta^{13}C$ values of dissolved inorganic carbon (DIC) of the global upper ocean via air-sea gas exchange. This process has been recently supported by model simulations (Shao et al., 2021). However, an eventual influence of oceanic

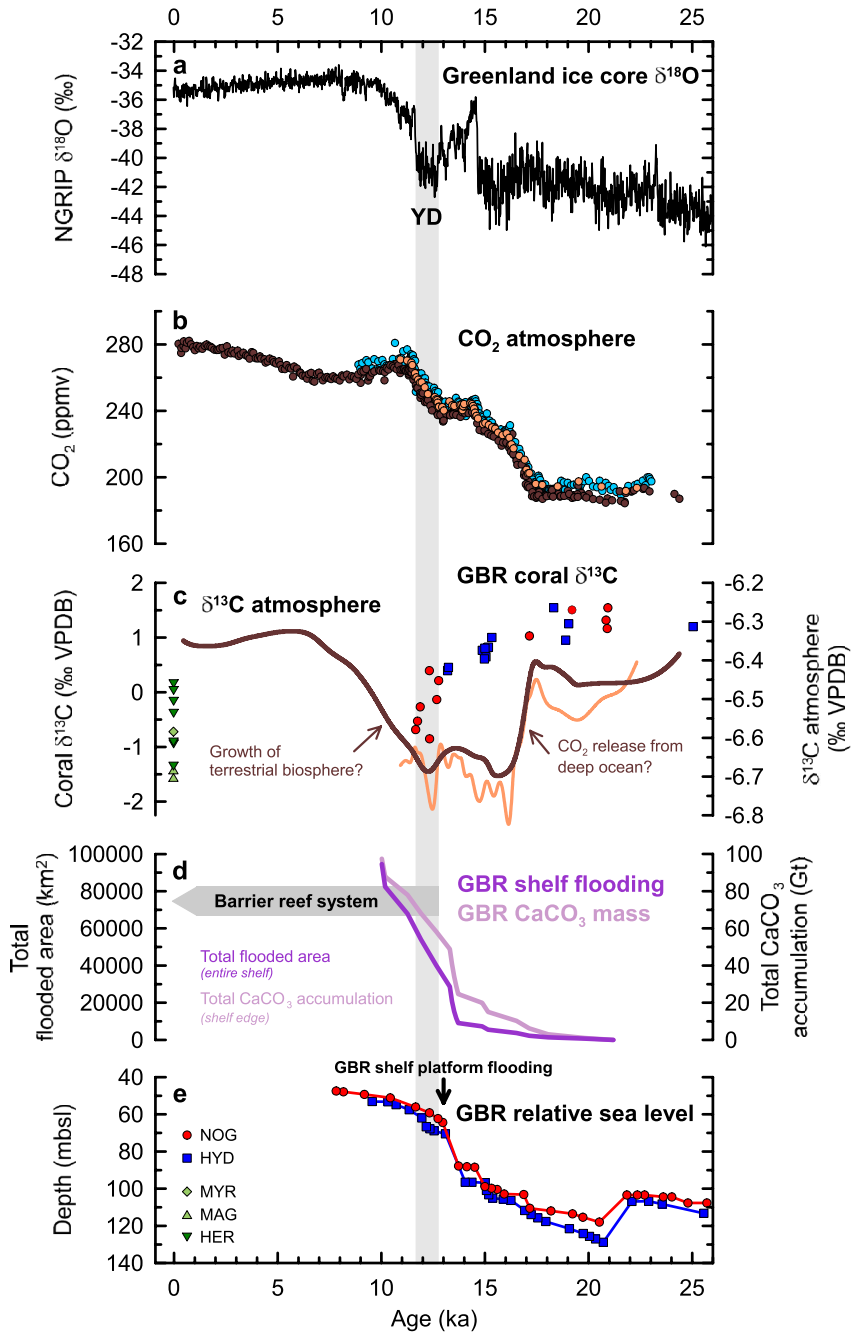

Figure 1. Great Barrier Reef (GBR) coral $\delta^{13}C$, shelf flooding, carbonate accumulation, sea level records and ice core records of atmospheric carbon. (a) Greenland ice core $\delta^{18}O$ record (North Greenland ice core project, NGRIP) (North Greenland Ice Core Project members, 2004), Younger Dryas (YD) cold event indicated. (b) Antarctic ice core reconstructions of atmospheric CO_2 (dark brown (Schmitt et al., 2012), light blue (Marcott et al., 2014), light brown (Bauska et al., 2016)). (c) Antarctic ice core reconstructions of $\delta^{13}C$ of atmospheric CO_2 (dark brown (Schmitt et al., 2012), Monte Carlo average; light brown (Bauska et al., 2016), smoothing spline). Mean skeletal $\delta^{13}C$ of GBR shallow-water corals (Felis et al., 2014a), anomalous 12.8 to 11.7 ka interval indicated (gray bar). Central GBR sites: Noggin Pass (NOG, red circle), Hydrographer's Passage (HYD, blue square), Myrmidon Reef (MYR, light green rhomb), Magnetic Island (MAG, light green triangle). Southern GBR site: Heron Island (HER, dark green triangle). (d) Calculated total (cumulative) marine-flooded area (Hinestrosa et al., 2019) (dark pink) at entire GBR shelf and reef carbonate ($CaCO_3$) accumulation (light pink) at shelf edge using sea level reconstructions (Webster et al., 2018; Yokoyama et al., 2018) from (e) (Text S1 in Supporting Information S1). (e) GBR maximum relative sea level reconstructions at NOG and HYD sites (Webster et al., 2018; Yokoyama et al., 2018). For uncertainties see original publications and Table S2 in Supporting Information S1.

changes in $\delta^{13}C_{DIC}$ values triggered by perturbations of the Atlantic meridional overturning circulation has also been suggested (Lund et al., 2019).

Overall, the late deglacial second minimum in atmospheric $\delta^{13}CO_2$ values has gained less attention compared to that observed during the early deglaciation, and its comprehensive explanation considering the complex interactions of all components of the past carbon cycle is still lacking. In this context, the development of shallow-water carbonate reefs, although acknowledged to be of relevance for the deglacial CO_2 rise (Brovkin et al., 2012; Ridgwell et al., 2003; Vecsei & Berger, 2004; W. H. Berger, 1982), has been usually neglected (Bauska et al., 2016; Schmitt et al., 2012). Carbon isotopic fractionation during calcium carbonate ($CaCO_3$) production is relatively small (Al-Rousan & Felis, 2013; Linsley et al., 2019; Swart et al., 2010) compared to fractionation during photosynthesis and, subsequently, little change in atmospheric $\delta^{13}CO_2$ is expected. However, to rigorously test this, precisely dated and well constrained reef carbonate records that span the last deglacial period are necessary, but such records are generally not available (Montaggioni, 2005).

A uranium-thorium (U-Th) dated record of coral skeletal $\delta^{13}C$ values from the Great Barrier Reef (Felis et al., 2014a; GBR), the world's largest contiguous coral reef system off northeastern Australia (Figure 2), shows a pronounced drop of 1.25‰ synchronous to the second minimum in atmospheric $\delta^{13}CO_2$ values at ~12.4 ka (Figure 1c) suggesting processes related to the growth of the "proto-GBR" that commenced at this time (Webster et al., 2018) might be at least partially responsible for the observed carbon cycle changes. Here, we combine these coral $\delta^{13}C$ values with other data from Integrated Ocean Drilling Program (IODP) Expedition 325 (Webster et al., 2011) reconstructing local sea level rise, shelf flooding, and reef carbonate accumulation for the last deglaciation (Webster et al., 2018; Yokoyama et al., 2018; Hinestrosa et al., 2019, 2022) in a carbon cycle modeling framework to investigate if and how both minima in $\delta^{13}C$ values are causally related to each other.

2. Last Deglacial GBR Coral $\delta^{13}C$ Record

The GBR record of coral $\delta^{13}C$ values (Figure 1c) is a stacked record from IODP drill sites at two locations, Noggin Pass (NOG) and Hydrographer's Passage (HYD; Figure 2). It is based on measurements of $\delta^{13}C$ values in the carbonate skeleton of U-Th dated *Isopora palifera/cuneata* colonies (Felis et al., 2014a). Twenty-five well-preserved fossil corals were recovered at depths between 56 and 126 m below present sea level in the central GBR (Figure 2), where they grew in shallow-water (0–10 m), high-energy reef crest environments during time intervals of the last deglaciation (Felis et al., 2014a; Text S1 in Supporting Information S1). In modern reef environments, skeletal $\delta^{13}C$ values of corals reflect the combined effects of various parameters including the availability of light for photosynthesis of the coral's algal symbionts, the coral's skeletal extension rate, and the autotrophy-heterotrophy ratio of the coral's diet (Al-Rousan & Felis, 2013; Felis et al., 1998; Gagan et al., 2015; Linsley et al., 2019; Suzuki et al., 2005; Swart, 1983; Swart et al., 1996c, 2005, 2010). These effects can result in a large range of skeletal $\delta^{13}C$ values, or intercolony variability, in corals derived from different parts of the same reef, as revealed by modern *Isopora palifera/cuneata* colonies from Heron Island (HER) in the southern GBR (Figures 1c and 2) (Felis et al., 2014a; Swart & Coleman, 1980). In addition to variations in skeletal $\delta^{13}C$ values that are mainly caused by metabolic responses of the corals to reef-scale differences in environmental conditions, basin-scale secular changes in surface ocean $\delta^{13}C_{DIC}$ are documented. The most compelling evidence for coral $\delta^{13}C$ values as a proxy for seawater $\delta^{13}C_{DIC}$ is provided by the imprint of the ^{13}C Suess effect (Keeling, 1979), the impact of anthropogenic CO_2 emissions with lower amounts of ^{13}C, on the $\delta^{13}C_{DIC}$ of the surface ocean (Al-Rousan & Felis, 2013; Dassié et al., 2013; Linsley et al., 2019; Swart et al., 2010). The magnitude of this decrease in surface water $\delta^{13}C_{DIC}$ can be modulated at a regional scale by input of terrestrial organic material with lower amounts of ^{13}C through runoff (Swart et al., 1996a, 1996b) and the complex interplay of photosynthesis and respiration during diurnal carbon cycling on shallow carbonate shelves (Geyman & Maloof, 2019; Text S1 in Supporting Information S1).

Importantly, the GBR record of coral $\delta^{13}C$ values does not reveal the typical w-shaped evolution observed in the last deglacial record of atmospheric $\delta^{13}CO_2$ values (Figure 1c). The record of coral $\delta^{13}C$ values does not document the first prominent minimum in atmospheric $\delta^{13}CO_2$ at ~16.0 ka as a result of the lack of suitable corals from this interval, but is largely consistent with the broad atmospheric $\delta^{13}CO_2$ minimum that commences after ~17 ka. The rather gentle decrease in coral $\delta^{13}C$ by about 0.5‰ between the ~21–17 ka interval and a cluster of corals at ~15 ka can be interpreted as an imprint of the atmospheric $\delta^{13}CO_2$ fall of similar magnitude on global

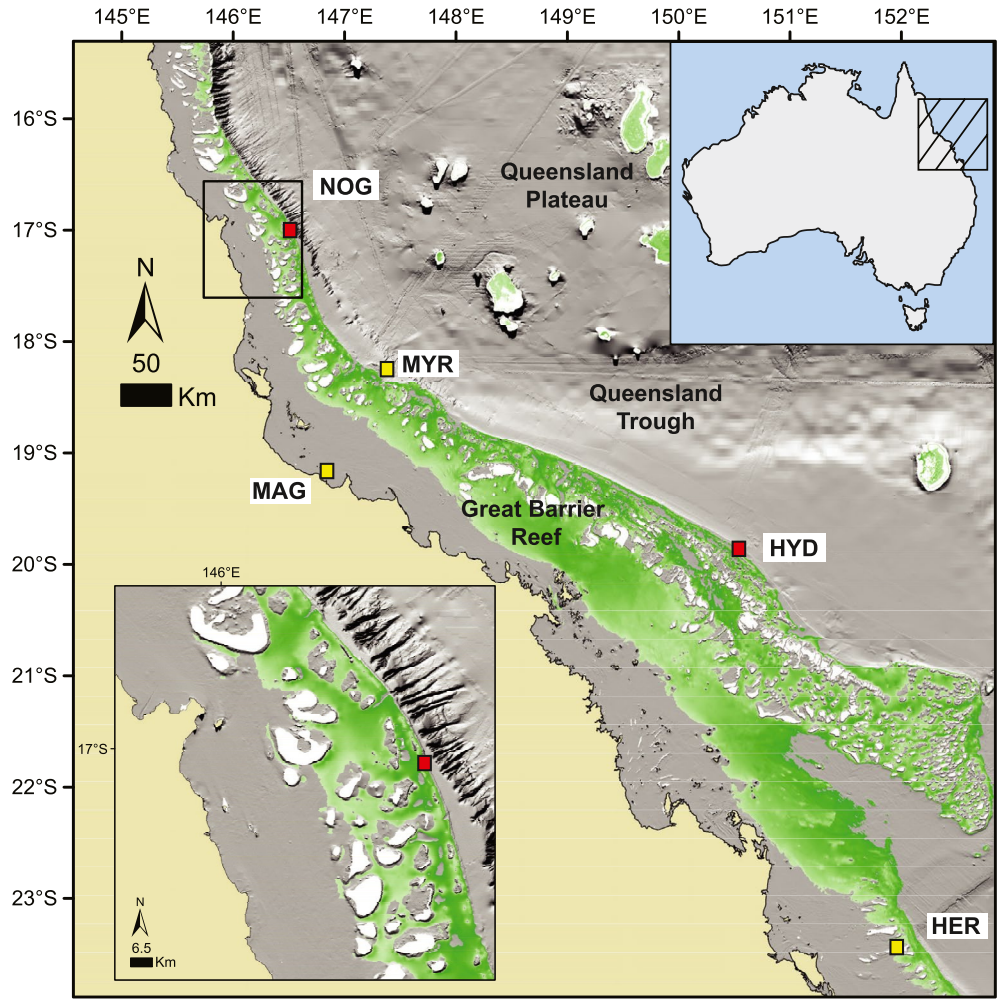

Figure 2. Map of the Great Barrier Reef (GBR) shelf. Flooded areas corresponding to sea levels between 45 and 75 m below present indicated (green) on present-day GBR bathymetry (Beaman, 2010). 45–75 m depth band shows extent of flooded terrestrial areas following 13.0 ka shelf platform flooding encompassing maximum range (depth and time) at which growth of "proto-GBR" (Reef 4) took place (Webster et al., 2018). Reef growth predominantly occurred along shelf edge seaward of modern GBR (Hinestrosa et al., 2019) (white areas). Not all flooded areas (green) were in situ reefs, but rather a variety of relatively shallow shelf settings. Locations of Integrated Ocean Drilling Program (IODP) Expedition 325 drilling sites at Noggin Pass (NOG) and Hydrographer's Passage (HYD) at central GBR shelf edge (Webster et al., 2011) (red squares). Modern coral sites at Heron Island (HER) (southern GBR) and Myrmidon Reef (MYR) and Magnetic Island (MAG) (central GBR) (yellow squares). Inset: Regional close-up of IODP site at NOG.

surface ocean $\delta^{13}C_{DIC}$ via air-sea gas exchange (Lynch-Stieglitz et al., 2019; Shao et al., 2021). This process is similar to the ^{13}C Suess effect (Keeling, 1979) and its imprint on surface ocean $\delta^{13}C_{DIC}$ and coral $\delta^{13}C$ today (Al-Rousan & Felis, 2013; Dassié et al., 2013; Linsley et al., 2019; Swart et al., 2010) and gives support to the use of GBR coral $\delta^{13}C$ values as proxy for surface ocean $\delta^{13}C_{DIC}$ changes during the last deglaciation. After another decrease of about 0.4‰ between ~15 and ~13 ka the most striking feature in the GBR record of coral $\delta^{13}C$ values is a pronounced decrease of up to 1.25‰ that occurred between 12.8 and 11.7 ka. The magnitude of this decrease in coral $\delta^{13}C$ is by far larger than the synchronous decline in atmospheric $\delta^{13}CO_2$ by 0.1–0.2‰ into its second prominent minimum centered at ~12.4 ka (Bauska et al., 2016; Schmitt et al., 2012), and points to processes intrinsic to the GBR (Figure 1c). Importantly, a potential influence of site-specific effects, intercolony variability, and changes in light availability, due to orbital insolation changes or a larger water depth of coral growth and/or increased reef water turbidity during the course of the last deglaciation, on the overall temporal evolution of the GBR record of coral $\delta^{13}C$ values, especially after 13.0 ka, can be largely ruled out (Text S1 in Supporting Information S1). While the overall trend in the record is considered as relatively robust given the uncertainty in

U-Th ages of ±100 years (Felis et al., 2014a), missing signals due to relatively sparse coral data during some time intervals, for example, prior to 21 ka, cannot be excluded.

3. GBR Shelf Flooding and Barrier Reef Initiation

Along the shelf off northeastern Australia, a substantial increase in marine flooded area and carbonate accumulation by coral reef organisms took place after 13.9 ka (Figure 1d). Between ~13.9 and 13.0 ka, a rapid sea-level rise (Figure 1e) and the availability of area for flooding favored coral reef growth along the shelf edge (Hinestrosa et al., 2019; Webster et al., 2018; Yokoyama et al., 2018). At 13.0 ka, the flooding of a large platform along the shelf (Figure 2), under a now slowly rising sea level (Hinestrosa et al., 2019; Webster et al., 2018; Yokoyama et al., 2018), marks a major change from narrow fringing reef systems to barrier-reef-dominated morphologies (Webster et al., 2018), which can be traced almost continuously over 2,000 km along the GBR shelf (Abbey et al., 2011; Hinestrosa et al., 2014), and which is immediately followed by the pronounced decrease in coral $\delta^{13}C$ values between 12.8 and 11.7 ka (Figure 1c). The extensive barrier reef system that initiated its growth along the shelf edge soon after the platform flooding was characterized by a thriving shallow-water (<5–10 m) coral community and is considered as the true "proto-GBR" (Webster et al., 2018). This reef represents one of the five distinct reef sequences in the IODP Expedition 325 GBR record of the past ~30 kyr, and is referred to as Reef 4 (Webster et al., 2018; Yokoyama et al., 2018). Prior to 13.0 ka, the shelf configuration had favored the formation of narrow fringing reefs (Webster et al., 2018). We estimate that between 13.9 and 13.0 ka an area of 25,160 km^2 was flooded and 293 Tmol of carbonate were accumulated mainly in shelf edge areas in the growing GBR (Figure 1d; Text S1 in Supporting Information S1), about 6-fold the amount of area flooded than during the 2 kyr before (15.9–13.9 ka). The total carbonate accumulation rose by a factor of 2.5 between both periods, however the annual carbonate accumulation rate increased from 57 to 326 Gmol yr^{-1}, while this rate when normalized per whole flooded area stayed with 13 mol yr^{-1} m^{-2} nearly constant (Table S1 in Supporting Information S1). From 13.0 to 11.7 ka another 24,590 km^2 was flooded on the wide shallow-water platform, leading to the accumulation of 181 Tmol of carbonate within the GBR reef system, mainly in shelf edge areas. The carbonate accumulation rate per whole flooded area dropped more than two-fold to 5.7 mol yr^{-1} m^{-2} after 13.0 ka (Table S1 in Supporting Information S1).

4. Carbon Cycle Modeling

Processes which might have led to the pronounced decrease in GBR coral $\delta^{13}C$ values after 13.0 ka (Figure 1c) are processes related to shelf platform flooding and changes in the coral's carbonate accumulation rate. Although largely variable the isotopic fractionation during carbonate production by reef corals (ε_{cor}) is on average reported to be slightly negative (Al-Rousan & Felis, 2013; Linsley et al., 2019; Swart et al., 2010). In our carbon cycle models, a 3-box model tailored for the specific situation of the GBR (Figure S1 in Supporting Information S1) and the global carbon cycle model BICYCLE (Köhler & Munhoven, 2020; Figure S2 and Text S1 in Supporting Information S1), we assume an ε_{cor} of −2‰, but test widely how this value and that of other parameters influence our results (Figure S3 and Text S1 in Supporting Information S1). The carbonate accumulation rate in the GBR normalized per area, if implemented in the 3-box carbon cycle model, is the relevant flux that determines the seawater $\delta^{13}C_{DIC}$. This rate was before 13.0 ka with 13 mol yr^{-1} m^{-2} and more (Table S1 in Supporting Information S1) responsible for an enrichment of seawater $\delta^{13}C_{DIC}$ of ~1.5‰ compared to a run without any coral reef growth (scenarios 100 and 000 in Figure 3a). At 13.0 ka the carbonate accumulation rate per whole flooded area dropped more than two-fold from 13.0 to 5.7 mol yr^{-1} m^{-2} (Table S1 in Supporting Information S1) drastically reducing the positive enrichment of regional seawater $\delta^{13}C_{DIC}$. This process alone can already explain a drop in $\delta^{13}C$ values of ~1.0‰, thus the dominant part of what is recorded in the corals between 12.8 and 11.7 ka (scenario 100 in Figure 3a; Text S1 in Supporting Information S1). When a similar carbonate sink via coral reef growth with identical isotopic fractionation is implemented into the surface equatorial Indo-Pacific box in the BICYCLE model (Text S1) such an enrichment of surface $\delta^{13}C_{DIC}$ leads to a small rise (nearly indistinguishable from zero) in simulated atmospheric $\delta^{13}CO_2$ and of +0.2 ppm in atmospheric CO_2 (Figure 4).

The decomposition (or respiration) of organic land carbon with lower amounts of ^{13}C on a newly flooded shelf platform, as has been suggested of relevance for other time periods (Köhler et al., 2011), potentially also contributed to the signal in $\delta^{13}C_{DIC}$ values of regional surface waters in the GBR during the last deglaciation. Implemented

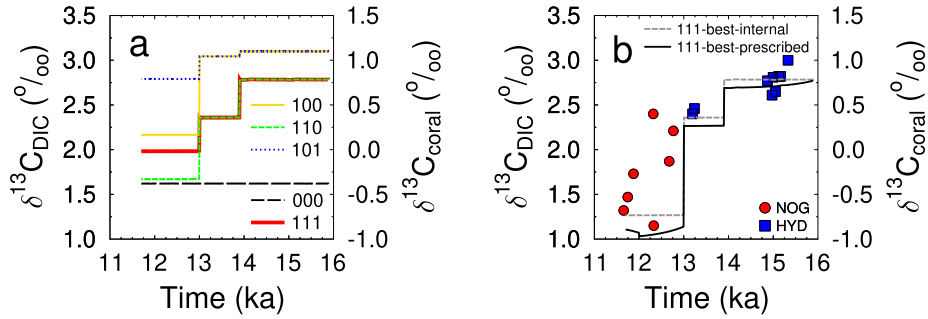

Figure 3. Contribution of different processes and best-guess results of 3-box carbon cycle model of Great Barrier Reef (GBR) growth. Simulated $\delta^{13}C$ values of seawater dissolved inorganic carbon (DIC) in GBR box, and of signal recorded by coral skeletons if an isotopic fractionation of −2‰ is assumed. (a) Scenarios follow a three-digit code showing 1 (on) or 0 (off), where the first digit states if coral carbonate accumulation, second digit if land carbon release after shelf flooding, and the third digit if changes in the water mixing between GBR box and open ocean at 13.0 ka is considered. (b) Two scenarios (prescribed vs. internally calculated atmospheric $\delta^{13}CO_2$) are shown with optimized (best-guess) parametrization (the amount of respired land carbon on flooded shelf assumed to raise from 30 kgC m^{-2} to 60 kgC m^{-2} at 13.0 ka). In the prescribed scenario, atmospheric $\delta^{13}CO_2$ is fixed for 15.9–13.0, 13.0–12.0, 12.0–11.7 ka at −6.6, −6.8, −6.6‰ following maximum amplitudes in Antarctic ice cores (Bauska et al., 2016), while in the internal scenario atmospheric $\delta^{13}CO_2$ is internally calculated in the model. For comparison, Integrated Ocean Drilling Program Expedition 325 GBR coral $\delta^{13}C$ data from Noggin Pass (NOG) and Hydrographer's Passage (HYD) are shown (Felis et al., 2014a).

in our modeling framework, an assumed land carbon density of 30 kgC m^{-2} (Köhler et al., 2005b) with a $\delta^{13}C$ value of −21‰ (Köhler et al., 2005a, 2011) released from the flooded areas, in general, shifts our simulation of seawater $\delta^{13}C_{DIC}$ toward smaller (less enriched) values (scenario 110 vs. 100 in Figure 3a and Figure S4a and S4b in Supporting Information S1). Around 13.9 ka, the about 6-fold increase in flooded area (Table S1 in Supporting Information S1), and therefore the higher decomposition rate of organic land carbon, leads to a drop in $\delta^{13}C_{DIC}$ by 0.5‰ (scenario 110 in Figure 3a and Figure S4b in Supporting Information S1). However, around 13.0 ka, this land carbon decomposition slightly dampens the drop in $\delta^{13}C_{DIC}$ caused by the reduced carbonate accumulation in corals by 0.2‰ (scenario 110 vs. 100 in Figure 3a and Figure S4a, S4b and Text S1 in Supporting Information S1). Following this process of land carbon decomposition, atmospheric CO_2 rose by another 0.1 ppm, while $\delta^{13}CO_2$ decreased by 0.001‰ in the global carbon cycle model simulations using the BICYCLE model (Figures 4b and 4c). Adding this process slightly reduces the enrichment effect of GBR carbonate accumulation on $\delta^{13}CO_2$, but the resulting anomaly is still positive (Figure 4c), opposite to the ice core reconstruction (Figure 1c).

Prior to 13.0 ka, the narrow fringing reefs that developed along the shelf slope can be considered as relatively well-flushed and exposed to rapid exchange of reef waters with the open ocean. In contrast, after 13.0 ka, the wide expanses of the flooded shallow-water platform bounded at the shelf edge by the growing barrier reef system (Hinestrosa et al., 2019; Webster et al., 2018) can be considered as less prone to rapid mixing with open-ocean waters. If implemented in our 3-box-model, a decrease in water exchange rates between the GBR and the open ocean at 13.0 ka leads to a reduction of the drop in $\delta^{13}C_{DIC}$ caused by the previously implemented processes (scenario 101 in Figure 3a and Figure S4c and Text S1 in Supporting Information S1).

If all three processes, isotopic fractionation during carbonate production, decomposition of flooded land carbon, and water exchange rates are active together they can potentially explain the observed coral $\delta^{13}C$ signal (scenario 111 in Figure 3a and Figure S4d in Supporting Information S1). The contribution of water exchange rates is rather minor here, and the explained amplitude seems to be with less than 1‰ still too small (Figure 3a). However, a closer match of the GBR record of coral $\delta^{13}C$ values with simulations is possible by some adjustments in the chosen parameter values, for example, by assuming that land carbon density was with 60 kgC/m^2 on the shelf platform twice as high as on the slope (best-guess scenarios shown in Figure 3b). This is in line with the substantially warmer conditions (Brenner et al., 2020; Felis et al., 2014a; Figure S5 in Supporting Information S1) and developing mangrove forests (Grindrod et al., 1999) after 13.0 ka in the GBR, and with estimates of combined tree, dead wood and soil carbon density of mangrove forests today (Donato et al., 2011; Sanderman et al., 2018). Furthermore, some fine-scale adjustments in the simulated coral $\delta^{13}C$ are obtained, when the variability of atmospheric $\delta^{13}CO_2$ is also taken into account (scenario "111-best-prescribed" in Figure 3b). This leads in $\delta^{13}C_{coral}$ to a

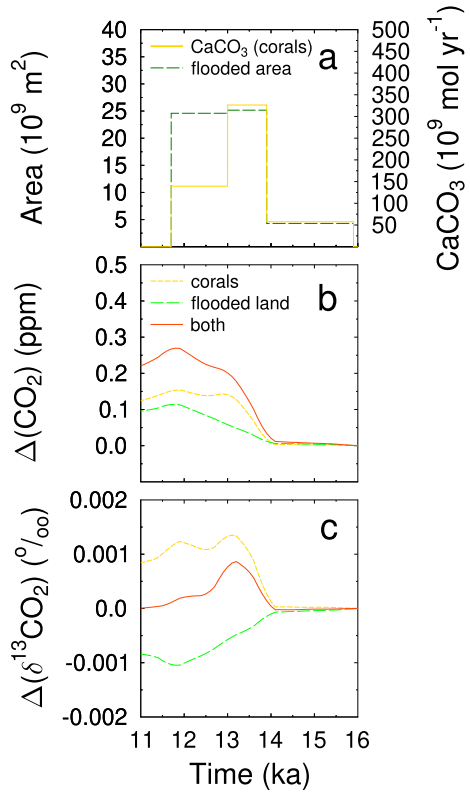

Figure 4. Results of global carbon cycle model with implemented Great Barrier Reef (GBR) growth. The carbon cycle model BICYCLE (Köhler & Munhoven, 2020) was used for the simulations. (a) Model forcing by the prescribed flooding of GBR shelf area and of coral carbonate ($CaCO_3$) production. Changes in atmospheric (b) CO_2 and (c) $\delta^{13}CO_2$ following three scenarios: (1) the prescribed accumulation of GBR coral carbonate with an isotopic fractionation during carbonate production of −2‰; (2) shelf flooding and release of CO_2 with $\delta^{13}C = -21‰$ from respired land carbon into the atmosphere assuming 30 kgC m^{-2} (15.9–13.0 ka) or 60 kgC m^{-2} (13.0–11.7 ka); (3) a combination of both.

drop by another 0.2‰ after 13 ka, allowing in principle for a smaller carbon release from flooded land than assumed so far.

5. Conclusions

Our modeling framework was able to identify the processes that were likely responsible for the last deglacial dynamics in $\delta^{13}C$ values observed in the GBR corals. The combination of isotopic fractionation during carbonate production and decomposition of flooded land carbon contributed to the dominant features of the record of coral $\delta^{13}C$ values, including the drop by 1.25‰ after 13.0 ka. Small variation of up to 0.2‰ from the imprint of changes in atmospheric $\delta^{13}CO_2$ values via air-sea gas exchange and a reduction in the simulated drop in $\delta^{13}C_{DIC}$ by reduced water exchange rates after 13.0 ka are only minor contributing processes. The nonlinear effect of the marine carbonate system, which via changing alkalinity and DIC concentrations alters the dissolved CO_2 concentration and thus the gas exchange rates, is essential for an understanding of these processes (Zeebe & Wolf-Gladrow, 2001). Therefore, this process identification can only be performed within a carbon cycle modeling framework. We note that extending the GBR record of *Isopora* coral $\delta^{13}C$ values to younger than 11.7 ka, supported by carbon cycle modeling, could provide further insights into the processes identified for the last deglaciation and their relative importance under changing Holocene boundary conditions.

The combined impact of both carbonate production and land carbon release from flooded areas in the GBR explains a deglacial rise in atmospheric CO_2 of 0.3 ppm only, and in atmospheric $\delta^{13}CO_2$ values of less than 0.001‰. Thus, the processes identified to be responsible for the large −1.25‰ anomaly in GBR coral $\delta^{13}C$ values between 12.8–11.7 ka did not contribute to the second prominent minimum in atmospheric $\delta^{13}CO_2$ values during the last deglaciation. The synchronicity of the $\delta^{13}C$ minima in both atmospheric CO_2 and GBR corals without one being largely responsible for the other should caution us to call for causal relationships without naming and quantifying a specific process.

Data Availability Statement

The coral data for this paper (Felis et al., 2014b) are available at https://doi.org/10.1594/PANGAEA.833408, and the Matlab/Octave code of the 3-box carbon cycle model and simulation results (Köhler et al., 2021), including shelf flooding and reef carbonate accumulation data as integrated in Figure 4a, are available at https://doi.pangaea.de/10.1594/PANGAEA.930114, at the World Data Center PANGAEA.

Acknowledgments
We acknowledge the International Ocean Discovery Program (IODP) and the European Consortium for Ocean Research Drilling (ECORD) for drilling the Great Barrier Reef (IODP Expedition 325 – Great Barrier Reef Environmental Changes). We thank H. Fischer, M. K. Gagan and H. Kuhnert for early discussions, reviewers for comments, and Expedition 325 scientists for contributions to previous publications. This work received funding from the Deutsche Forschungsgemeinschaft (DFG, German Research Foundation) - project number 180346848, through Priority Programme 527 "IODP". Financial support was also provided by the Australian Research Council (grant no. DP1094001). Open access funding enabled and organized by Projekt DEAL.

References

Abbey, E., Webster, J. M., & Beaman, R. J. (2011). Geomorphology of submerged reefs on the shelf edge of the Great Barrier Reef: The influence of oscillating Pleistocene sea-levels. *Marine Geology*, *288*(1–4), 61–78. https://doi.org/10.1016/j.margeo.2011.08.006

Al-Rousan, S., & Felis, T. (2013). Long-term variability in the stable carbon isotopic composition of *Porites* corals at the northern Gulf of Aqaba, Red Sea. *Palaeogeography, Palaeoclimatology, Palaeoecology*, *381–382*, 1–14. https://doi.org/10.1016/j.palaeo.2013.03.025

Anderson, R. F., Ali, S., Bradtmiller, L. I., Nielsen, S. H. H., Fleisher, M. Q., Anderson, B. E., & Burckle, L. H. (2009). Wind-driven upwelling in the southern ocean and the deglacial rise in atmospheric CO_2. *Science*, *323*(5920), 1443–1448. https://doi.org/10.1126/science.1167441

Bauska, T. K., Baggenstos, D., Brook, E. J., Mix, A. C., Marcott, S. A., Petrenko, V. V., et al. (2016). Carbon isotopes characterize rapid changes in atmospheric carbon dioxide during the last deglaciation. *Proceedings of the National Academy of Sciences*, *113*(13), 3465–3470. https://doi.org/10.1073/pnas.1513868113

Beaman, R. J. (2010). Project 3DGBR: A high-resolution depth model for the Great barrier reef and coral sea. In *Plus Appendix pp*. Reef and Rainforest Research Centre.Rep. Marine and tropical sciences Research facility (MTSRF) Project 2.5i.1a Final Report 13.

Berger, W. H. (1982). Increase of carbon dioxide in the atmosphere during deglaciation: The coral reef hypothesis. *Naturwissenschaften*, *69*(2), 87–88. https://doi.org/10.1007/BF00441228

Böhm, E., Lippold, J., Gutjahr, M., Frank, M., Blaser, P., Antz, B., et al. (2015). Strong and deep Atlantic meridional overturning circulation during the last glacial cycle. *Nature*, *517*(7532), 73–76. https://doi.org/10.1038/nature14059

Brenner, L. D., Linsley, B. K., Webster, J. M., Potts, D., Felis, T., Gagan, M. K., et al. (2020). Coral record of Younger Dryas chronozone warmth on the Great Barrier Reef. *Paleoceanography and Paleoclimatology*, *35*(12), e2020PA003962. https://doi.org/10.1029/2020PA003962

Brovkin, V., Ganopolski, A., Archer, D., & Munhoven, G. (2012). Glacial CO_2 cycle as a succession of key physical and biogeochemical processes. *Climate of the Past*, *8*(1), 251–264. https://doi.org/10.5194/cp-8-251-2012

Dassié, E. P., Lemley, G. M., & Linsley, B. K. (2013). The Suess effect in Fiji coral $\delta^{13}C$ and its potential as a tracer of anthropogenic CO_2 uptake. *Palaeogeography, Palaeoclimatology, Palaeoecology*, *370*, 30–40. https://doi.org/10.1016/j.palaeo.2012.11.012

Donato, D. C., Kauffman, J. B., Murdiyarso, D., Kurnianto, S., Stidham, M., & Kanninen, M. (2011). Mangroves among the most carbon-rich forests in the tropics. *Nature Geoscience*, *4*(5), 293–297. https://doi.org/10.1038/ngeo1123

Felis, T., McGregor, H. V., Linsley, B. K., Tudhope, A. W., Gagan, M. K., Suzuki, A., et al. (2014a). Intensification of the meridional temperature gradient in the Great Barrier Reef following the Last Glacial Maximum. *Nature Communications*, *5*, 4102. https://doi.org/10.1038/ncomms5102

Felis, T., McGregor, H. V., Linsley, B. K., Tudhope, A. W., Gagan, M. K., Suzuki, A., et al. (2014b). Great Barrier Reef coral element/Ca and stable isotope data and U-Th ages from IODP Expedition 325 dataset [dataset]. PANGAEA. https://doi.org/10.1594/PANGAEA.833408

Felis, T., Pätzold, J., Loya, Y., & Wefer, G. (1998). Vertical water mass mixing and plankton blooms recorded in skeletal stable carbon isotopes of a Red Sea coral. *Journal of Geophysical Research*, *103*(C13), 30731–30739. https://doi.org/10.1029/98JC02711

Gagan, M. K., Sosdian, S. M., Scott-Gagan, H., Sieh, K., Hantoro, W. S., Natawidjaja, D. H., et al. (2015). Coral $^{13}C/^{12}C$ records of vertical seafloor displacement during megathrust earthquakes west of Sumatra. *Earth and Planetary Science Letters*, *432*, 461–471. https://doi.org/10.1016/j.epsl.2015.10.002

Geyman, E. C., & Maloof, A. C. (2019). A diurnal carbon engine explains ^{13}C-enriched carbonates without increasing the global production of oxygen. *Proceedings of the National Academy of Sciences*, *116*(49), 24433–24439. https://doi.org/10.1073/pnas.1908783116

Gottschalk, J., Battaglia, G., Fischer, H., Frölicher, T. L., Jaccard, S. L., Jeltsch-Thömmes, A., et al. (2019). Mechanisms of millennial-scale atmospheric CO_2 change in numerical model simulations. *Quaternary Science Reviews*, *220*, 30–74. https://doi.org/10.1016/j.quascirev.2019.05.013

Grindrod, J., Moss, P., & Kaars, S. V. D. (1999). Late quaternary cycles of mangrove development and decline on the north Australian continental shelf. *Journal of Quaternary Science*, *14*(5), 465–470. https://doi.org/10.1002/(SICI)1099-1417(199908)14:5%3C465::AID-JQS473%3E3.0

Hinestrosa, G., Webster, J. M., & Beaman, R. J. (2016). Postglacial sediment deposition along a mixed carbonate-siliciclastic margin: New constraints from the drowned shelf-edge reefs of the Great Barrier Reef, Australia. *Palaeogeography, Palaeoclimatology, Palaeoecology*, *446*, 168–185. https://doi.org/10.1016/j.palaeo.2016.01.023

Hinestrosa, G., Webster, J. M., & Beaman, R. J. (2019). Spatio-temporal patterns in the postglacial flooding of the Great Barrier Reef shelf, Australia. *Continental Shelf Research*, *173*, 13–26. https://doi.org/10.1016/j.csr.2018.12.001

Hinestrosa, G., Webster, J. M., & Beaman, R. J. (2022). New constraints on the postglacial shallow-water carbonate accumulation in the Great Barrier Reef. *Scientific Reports*, *12*, 924. https://doi.org/10.1038/s41598-021-04586-w

Hinestrosa, G., Webster, J. M., Beaman, R. J., & Anderson, L. M. (2014). Seismic stratigraphy and development of the shelf-edge reefs of the Great Barrier Reef, Australia. *Marine Geology*, *353*, 1–20. https://doi.org/10.1016/j.margeo.2014.03.016

Keeling, C. D. (1979). The suess effect: ^{13}Carbon-^{14}Carbon interrelations. *Environment International*, *2*(4), 229–300. https://doi.org/10.1016/0160-4120(79)90005-9

Köhler, P., Felis, T., Hinestrosa, G., & Webster, J. M. (2021). Simulation results for the role of the deglacial buildup of the Great Barrier Reef for the global carbon cycle, [dataset], Retrieved from https://doi.pangaea.de/10.1594/PANGAEA.930114

Köhler, P., Fischer, H., Munhoven, G., & Zeebe, R. E. (2005a). Quantitative interpretation of atmospheric carbon records over the last glacial termination. *Global Biogeochemical Cycles*, *19*(4), GB4020. https://doi.org/10.1029/2004GB002345

Köhler, P., Joos, F., Gerber, S., & Knutti, R. (2005b). Simulated changes in vegetation distribution, land carbon storage, and atmospheric CO_2 in response to a collapse of the North Atlantic thermohaline circulation. *Climate Dynamics*, *25*(7), 689–708. https://doi.org/10.1007/s00382-005-0058-8

Köhler, P., Knorr, G., Buiron, D., Lourantou, A., & Chappellaz, J. (2011). Abrupt rise in atmospheric CO_2 at the onset of the Bølling/Allerød: In-situ ice core data versus true atmospheric signals. *Climate of the Past*, *7*(2), 473–486. https://doi.org/10.5194/cp-7-473-2011

Köhler, P., & Munhoven, G. (2020). Late Pleistocene carbon cycle revisited by considering solid earth processes. *Paleoceanography and Paleoclimatology*, *35*(12), e2020PA004020. https://doi.org/10.1029/2020PA004020

Linsley, B. K., Dunbar, R. B., Dassié, E. P., Tangri, N., Wu, H. C., Brenner, L. D., & Wellington, G. M. (2019). Coral carbon isotope sensitivity to growth rate and water depth with paleo-sea level implications. *Nature Communications*, *10*, 2056. https://doi.org/10.1038/s41467-019-10054-x

Lund, D., Hertzberg, J., & Lacerra, M. (2019). Carbon isotope minima in the south Atlantic during the last deglaciation: Evaluating the influence of air-sea gas exchange. *Environmental Research Letters*, *14*(5), 055004. https://doi.org/10.1088/1748-9326/ab126f

Lynch-Stieglitz, J., Valley, S. G., & Schmidt, M. W. (2019). Temperature-dependent ocean–atmosphere equilibration of carbon isotopes in surface and intermediate waters over the deglaciation. *Earth and Planetary Science Letters*, *506*, 466–475. https://doi.org/10.1016/j.epsl.2018.11.024

Marchitto, T. M., Lehman, S. J., Ortiz, J. D., Flückiger, J., & van Geen, A. (2007). Marine radiocarbon evidence for the mechanism of deglacial atmospheric CO_2 rise. *Science*, *316*(5830), 1456–1459. https://doi.org/10.1126/science.1138679

Marcott, S. A., Bauska, T. K., Buizert, C., Steig, E. J., Rosen, J. L., Cuffey, K. M., et al. (2014). Centennial-scale changes in the global carbon cycle during the last deglaciation. *Nature*, *514*, 616–619. https://doi.org/10.1038/nature13799

Menviel, L., Spence, P., Yu, J., Chamberlain, M. A., Matear, R. J., Meissner, K. J., & England, M. H. (2018). Southern Hemisphere westerlies as a driver of the early deglacial atmospheric CO_2 rise. *Nature Communications*, *9*, 2503. https://doi.org/10.1038/s41467-018-04876-4

Montaggioni, L. F. (2005). History of Indo-Pacific coral reef systems since the last glaciation: Development patterns and controlling factors. *Earth-Science Reviews*, *71*(1), 1–75. https://doi.org/10.1016/j.earscirev.2005.01.002

Ridgwell, A. J., Watson, A. J., Maslin, M. A., & Kaplan, J. O. (2003). Implications of coral reef buildup for the controls on atmospheric CO_2 since the Last Glacial Maximum. *Paleoceanography*, *18*(4), 1083. https://doi.org/10.1029/2003PA000893

Ronge, T. A., Prange, M., Mollenhauer, G., Ellinghausen, M., Kuhn, G., & Tiedemann, R. (2020). Radiocarbon evidence for the contribution of the southern Indian Ocean to the evolution of atmospheric CO_2 over the last 32,000 years. *Paleoceanography and Paleoclimatology*, *35*(3), e2019PA003733. https://doi.org/10.1029/2019PA003733

Sanderman, J., Hengl, T., Fiske, G., Solvik, K., Adame, M. F., Benson, L., et al. (2018). A global map of mangrove forest soil carbon at 30 m spatial resolution. *Environmental Research Letters*, *13*(5), 055002. https://doi.org/10.1088/1748-9326/aabe1c

Schmitt, J., Schneider, R., Elsig, J., Leuenberger, D., Lourantou, A., Chappellaz, J., et al. (2012). Carbon isotope constraints on the deglacial CO_2 rise from ice cores. *Science*, *336*(6082), 711–714. https://doi.org/10.1126/science.1217161

Shao, J., Stott, L. D., Menviel, L., Ridgwell, A., Ödalen, M., & Mohtadi, M. (2021). The atmospheric bridge communicated the $\delta^{13}C$ decline during the last deglaciation to the global upper ocean. *Climate of the Past*, *17*(4), 1507–1521. https://doi.org/10.5194/cp-17-1507-2021

Shuttleworth, R., Bostock, H. C., Chalk, T. B., Calvo, E., Jaccard, S. L., Pelejero, C., et al. (2021). Early deglacial CO_2 release from the sub-Antarctic Atlantic and Pacific oceans. *Earth and Planetary Science Letters*, *554*, 116649. https://doi.org/10.1016/j.epsl.2020.116649

Skinner, L. C., Fallon, S., Waelbroeck, C., Michel, E., & Barker, S. (2010). Ventilation of the deep southern ocean and deglacial CO_2 rise. *Science*, *328*(5982), 1147–1151. https://doi.org/10.1126/science.1183627

Suzuki, A., Hibino, K., Iwase, A., & Kawahata, H. (2005). Intercolony variability of skeletal oxygen and carbon isotope signatures of cultured Porites corals: Temperature-controlled experiments. *Geochimica et Cosmochimica Acta*, *69*(18), 4453–4462. https://doi.org/10.1016/j.gca.2005.05.018

Swart, P. K. (1983). Carbon and oxygen isotope fractionation in scleractinian corals: A review. *Earth-Science Reviews*, *19*(1), 51–80. https://doi.org/10.1016/0012-8252(83)90076-4

Swart, P. K., & Coleman, M. L. (1980). Isotopic data for scleractinian corals explain their palaeotemperature uncertainties. *Nature*, *283*(5747), 557–559. https://doi.org/10.1038/283557a0

Swart, P. K., Dodge, R. E., & Hudson, H. J. (1996a). A 240-year stable oxygen and carbon isotopic record in a coral from South Florida; implications for the prediction of precipitation in southern Florida. *PALAIOS*, *11*(4), 362–375. https://doi.org/10.2307/3515246

Swart, P. K., Greer, L., Rosenheim, B. E., Moses, C. S., Waite, A. J., Winter, A., et al. (2010). The ^{13}C Suess effect in scleractinian corals mirror changes in the anthropogenic CO_2 inventory of the surface oceans. *Geophysical Research Letters*, *37*(5), L05604. https://doi.org/10.1029/2009GL041397

Swart, P. K., Healy, G. F., Dodge, R. E., Kramer, P., Hudson, J. H., Halley, R. B., & Robblee, M. B. (1996b). The stable oxygen and carbon isotopic record from a coral growing in Florida Bay: A 160 year record of climatic and anthropogenic influence. *Palaeogeography, Palaeoclimatology, Palaeoecology*, *123*(1), 219–237. https://doi.org/10.1016/0031-0182(95)00078-X

Swart, P. K., Szmant, A., Porter, J. W., Dodge, R. E., Tougas, J. I., & Southam, J. R. (2005). The isotopic composition of respired carbon dioxide in scleractinian corals: Implications for cycling of organic carbon in corals. *Geochimica et Cosmochimica Acta*, *69*(6), 1495–1509. https://doi.org/10.1016/j.gca.2004.09.004

Swart, P. K., Szmant, A. M., & Dodge, R. E. (1996c). The origin of variations in the isotopic record of scleractinian corals: II. Carbon. *Geochimica et Cosmochimica Acta*, *60*(15), 2871–2885. https://doi.org/10.1016/0016-7037(96)00119-6

Vecsei, A., & Berger, W. H. (2004). Increase of atmospheric CO_2 during deglaciation: Constraints on the coral reef hypothesis from patterns of deposition. *Global Biogeochemical Cycles*, *18*(1), GB1035. https://doi.org/10.1029/2003GB002147

Webster, J. M., Braga, J. C., Humblet, M., Potts, D. C., Iryu, Y., Yokoyama, Y., et al. (2018). Response of the Great Barrier Reef to sea-level and environmental changes over the past 30,000 years. *Nature Geoscience*, *11*, 426–432. https://doi.org/10.1038/s41561-018-0127-3

Webster, J. M., Yokoyama, Y., Cotteril, C., & Expedition 325 Scientists (2011). *Proc. IODP, 325*. Integrated Ocean Drilling Program Management International, Inc. https://doi.org/10.2204/iodp.proc.325.2011

Yokoyama, Y., Esat, T. M., Thompson, W. G., Thomas, A. L., Webster, J. M., Miyairi, Y., et al. (2018). Rapid glaciation and a two-step sea level plunge into the Last Glacial Maximum. *Nature*, *559*, 603–607. https://doi.org/10.1038/s41586-018-0335-4

Zeebe, R. E., & Wolf-Gladrow, D. (2001). *CO_2 in seawater: Equilibrium, kinetics, isotopes*. Elsevier.346.

References From the Supporting Information

Berger, A. L. (1978). Long-term variations of daily insolation and Quaternary climatic changes. *Journal of the Atmospheric Sciences*, *35*, 2362–2367. https://doi.org/10.1175/1520-0469(1978)035%3C2362:LTVODI%3E2.0

DeLong, K. L., Quinn, T. M., Shen, C.-C., & Lin, K. (2010). A snapshot of climate variability at Tahiti at 9.5 ka using a fossil coral from IODP Expedition 310. *Geochemistry, Geophysics, Geosystems*, *11*(6), Q06005. https://doi.org/10.1029/2009GC002758

Dunbar, G. B., & Dickens, G. R. (2003). Massive siliciclastic discharge to slopes of the Great Barrier Reef platform during sea-level transgression: Constraints from sediment cores between 15°S and 16°S latitude and possible explanations. *Sedimentary Geology*, *162*(1), 141–158. https://doi.org/10.1016/S0037-0738(03)00216-1

Felis, T., Suzuki, A., Kuhnert, H., Dima, M., Lohmann, G., & Kawahata, H. (2009). Subtropical coral reveals abrupt early-twentieth-century freshening in the western North Pacific Ocean. *Geology*, *37*(6), 527–530. https://doi.org/10.1130/G25581A.1

Gagan, M. K., Dunbar, G. B., & Suzuki, A. (2012). The effect of skeletal mass accumulation in *Porites* on coral Sr/Ca and $\delta^{18}O$ paleothermometry. *Paleoceanography*, *27*, PA1203. https://doi.org/10.1029/2011PA002215

Harris, P. T., Bridge, T. C. L., Beaman, R. J., Webster, J. M., Nichol, S. L., & Brooke, B. P. (2012). Submerged banks in the Great Barrier Reef, Australia, greatly increase available coral reef habitat. *ICES Journal of Marine Science*, *70*(2), 284–293. https://doi.org/10.1093/icesjms/fss165

Humblet, M., Potts, D. C., Webster, J. M., Braga, J. C., Iryu, Y., Yokoyama, Y., et al. (2019). Late glacial to deglacial variation of coralgal assemblages in the Great Barrier Reef, Australia. *Global and Planetary Change*, *174*, 70–91. https://doi.org/10.1016/j.gloplacha.2018.12.014

Köhler, P., Fischer, H., & Schmitt, J. (2010). Atmospheric $\delta^{13}CO_2$ and its relation to pCO_2 and deep ocean $\delta^{13}C$ during the late Pleistocene. *Paleoceanography*, *25*(1), PA1213. https://doi.org/10.1029/2008PA001703

Kojis, B. L., & Quinn, N. J. (1984). Seasonal and depth variation in fecundity of *Acropora palifera* at two reefs in Papua New Guinea. *Coral Reefs*, *3*(3), 165–172. https://doi.org/10.1007/BF00301961

Lambeck, K., Rouby, H., Purcell, A., Sun, Y., & Sambridge, M. (2014). Sea level and global ice volumes from the last glacial maximum to the Holocene. *Proceedings of the National Academy of Sciences*, *111*(43), 15296–15303. https://doi.org/10.1073/pnas.1411762111

Locarnini, R. A., Mishonov, A. V., Antonov, J. I., Boyer, T. P., Garcia, H. E., Baranova, O. K., et al. (2010). World Ocean Atlas 2009, volume 1: Temperature. *NOAA Atlas NESDIS*, *68*, 184.

Mongin, M., Baird, M. E., Tilbrook, B., Matear, R. J., Lenton, A., Herzfeld, M., et al. (2016). The exposure of the Great Barrier Reef to ocean acidification. *Nature Communications*, *7*, 10732. https://doi.org/10.1038/ncomms10732

Mook, W. G. (1986). ^{13}C in atmospheric CO_2. *Netherlands Journal of Sea Research*, *20*(2), 211–223. https://doi.org/10.1016/0077-7579(86)90043-8

North Greenland Ice Core Project members. (2004). High-resolution record of northern hemisphere climate extending into the last interglacial period. *Nature*, *431*(7005), 147–151. https://doi.org/10.1038/nature02805

Page, M. C., & Dickens, G. R. (2005). Sediment fluxes to Marion Plateau (southern Great Barrier Reef province) over the last 130 ky: New constraints on "transgressive-shedding" off northeastern Australia. *Marine Geology*, *219*(1), 27–45. https://doi.org/10.1016/j.margeo.2005.05.002